Available online at www.sciencedirect.com
ScienceDirect
International Journal of Heat and Mass Transfer 50 (2007) 2161–2169
International Journal of HEAT and MASS TRANSFER
www.elsevier.com/locate/ijhmt

Analysis of melting of alloy powder bed with constant heat flux

Bin Xiao, Yuwen Zhang *

Department of Mechanical and Aerospace Engineering, University of Missouri-Columbia, Columbia, MO 65211, USA

Received 13 March 2006; received in revised form 5 November 2006
Available online 11 January 2007

Abstract

Melting of an alloy powder bed with constant heat flux for application in selective laser sintering (SLS) is analyzed in this paper. Since melting of an alloy occurs in a range of temperatures, instead of at a single melting point, there will be a mushy zone – containing partially melted powders – between the unmelted region and the completely melted region. The mushy zone can be further divided into two sub-regions: (1) a lower part with constant porosity (shrinkage takes place), and (2) an upper part with constant volume (no shrinkage). Temperature distributions in different regions and locations of melting interfaces are obtained using an integral approximation method. The results show that increasing initial porosity and temperature of the powder bed accelerate the melting process. The melting slows down with increasing thermal conductivity of the interstitial gas.

1. Introduction

Direct metal laser sintering (DMLS) is a rapid prototyping/manufacturing technology, which directly fabricates parts via melting and resolidification of metallic powders [1–5]. Fundamentals of heat transfer in melting and solidification have been studied intensively and are well documented [6–8]. Carslaw and Jaeger [9] discussed melting of a semi-infinite body with constant thermophysical properties, and obtained an analytical solution for Dirichlet boundary conditions. Lax [10] studies the temperature rise under a steady-state condition due to a stationary Gaussian beam in a semi-infinite cylindrical medium. Bell [11] developed a one-dimensional thermal model for laser annealing over a wide range of laser pulse duration and absorption coefficient. Yilbas [12] has presented a numerical solution for a pulsed CO_2 laser heating process. Rostaml and Raisi [13] have numerically solved the temperature distribution and melt pool size in a semi-infinite body due to a moving laser heat source. Kim and Sim [14] have studied thermal behavior and fluid flow during laser surface heating of alloys. Iwamoto et al. [15] have performed numerical analysis of energy transfer and surface modification of a metal surface by pulsed laser heating. While the above studies focused on long-pulse laser-material interactions, phase change heat transfer during ultrashort laser processing of metal films has also been investigated [16,17]. The thermal contact resistance between the mold and substrate during laser-assisted imprinting fabrication was numerically investigated by Hsiao et al. [18].

During the DMLS process, the powder bed shrinks as the porosity of the powder bed becomes nearly zero after melting. The effect of shrinkage during solid–liquid phase change processes has been investigated by some researchers. Eckert and Drake [19] obtained a similarity solution of a one-dimensional solidification problem with the consideration of the density change in phase change. Zhang and Faghri [20] analytically solved a one-dimensional melting problem in a powder bed containing a powder mixture under a boundary condition of the second kind. The results showed that the shrinkage effect on the melting of the powder bed is not negligible. Konrad et al. [21] obtained an analytical solution of melting and resolidification of a two-component metal powder bed subjected to temporal Gaussian heat flux. Xiao and Zhang [22] analytically solved

* Corresponding author. Tel.: +1 573 884 6936; fax: +1 573 884 5090.
E-mail address: zhangyu@missouri.edu (Y. Zhang).

0017-9310/$ - see front matter © 2006 Elsevier Ltd. All rights reserved.
doi:10.1016/j.ijheatmasstransfer.2006.11.012

Nomenclature

c	specific heat (J/kg K)
f	mass fraction of solid
f_0	mass fraction of solid on the heating surface
$h_{s\ell}$	latent heat of melting (J/kg)
k	thermal conductivity (W/m K)
K	dimensionless thermal conductivity
q''	heat flux absorbed by the powder bed (W/m^2)
s_0	location of heating surface (m)
s_m	location of interface between upper and lower parts of mushy zone (m)
s_ℓ	location of interface between liquid and mushy zones (m)
s	location of interface between solid and mushy zones (m)
S_0	dimensionless location of heating surface
S_m	dimensionless location of interface between upper and lower parts of mushy zone
S_ℓ	dimensionless location of interface between liquid and mushy zones
S	dimensionless location of interface between solid and mushy zone
T_i	initial temperature on the powder bed
T	temperature (K)
$T_{\ell m}$	liquidus temperature (K)
T_{sm}	solidus temperature (K)
t	time (s)
V	volume (m^3)
w	shrinkage velocity (m/s)
W	dimensionless shrinkage velocity
z	vertical coordinate (m)
Z	dimensionless vertical coordinate

Greek symbols

α	thermal diffusivity (m^2 s)
α_0	weighted average in the function for calculating effective thermal conductivity of the powder bed
δ	powder thermal penetration depth (m)
$\delta\theta$	dimensionless melting temperature range
θ	dimensionless temperature
Δ	dimensionless thermal penetration depth
ε	porosity (volume fraction of void), $(V_g + V_\ell)/(V_g + V_\ell + V_s)$
ρ	density (kg/m^3)
τ	dimensionless time
φ_g	volume fraction of gas, $V_g/(V_g + V_\ell + V_s)$
φ_ℓ	volume fraction of liquid, $V_\ell/(V_g + V_\ell + V_s)$
φ_s	volume fraction of solid, $V_s/(V_g + V_\ell + V_s)$

Subscripts

0	surface
eff	effective
g	gas
f	fusion
i	initial
ℓ	liquid
m	mushy zone
p	metal powder
s	solid

rapid melting of a subcooled single-component metal powder bed in the SLS process. Under irradiation of a pulse laser beam, the surface of the powder particle is molten first and the core of the particle remains solid. Melting in SLS of single-component metal powder was modeled as melting occurring in a range of temperature with significant density change.

In contrast to metals with well-defined melting point, alloyed powders exhibits a melting temperature range during the sintering process. Therefore, mushy zone containing mixture of liquid and solid is formed, and the temperature in the mushy zone is between solidus and liquidus temperatures. Niu and Chang [23] showed that during the DMLS of high-speed steel powders, a liquid phase forms along the grain boundaries in the particles. The liquid flows and wets the solid particles or the grain boundaries. This results in rapid densification by rearrangement of the solid particles. Prabhu and Bourell reported similar mechanism in the DMLS of pre-alloyed bronze powders [24].

Before DMLS of alloy powders, the powder structure is supported by the solid particles. Partial melting of the powder particle during DMLS will result in decrease of the powder bed volume because the void spaces initially occupied by the gas will be taken up by the liquid phase. Conservation of mass principles shows that the porosity of the powder bed, defined as summation of the volume fraction of the gas and liquid, remains constant (while the volume of the powder bed shrinks) [25]. When all gas is driven out, the shrinkage process ceases and the volume of the powder will be constant from that moment. Therefore, the mushy zone between the liquid region and solid region can be further divided into two parts: the lower part with constant porosity and the upper part with constant volume.

In order to understand the mechanisms of DMLS of alloy powders, melting of alloy powder bed with shrinkage phenomena will be investigated in this paper. The temperature distribution and locations of melting interfaces will be obtained using an integral approximation method. Effects of processing parameters such as porosity, subcooling parameters, and thermal conductivity of the interstitial gas(es) on melting process will be investigated.

2. Physical model

The problem under consideration is shown in Fig. 1. A randomly packed metal powder bed, which is initially at a

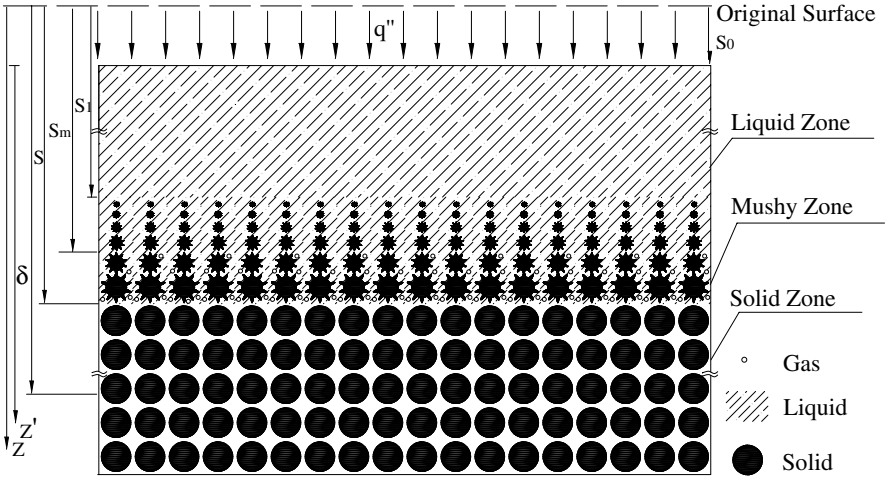

Fig. 1. Physical model of direct metal laser sintering with constant heat flux.

uniform temperature, T_i, below the solidus temperature of the powders, T_{sm}, is in a half space, $z > 0$. At time $t = 0$, a constant heat flux, q'', is applied to the surface of the powder bed. Since alloy powders melt in a range of temperature $(T_{sm}, T_{\ell m})$, a mushy zone is formed when the surface temperature of the powder bed reaches the solidus temperature. The mushy zone can be divided into two sub-regions depending on whether shrinkage is accompanied: (1) lower part with constant porosity (shrinkage takes place), and (2) upper part with constant volume (no shrinkage). The melting of alloy powders is accomplished in three stages. During the first stage, the lower part of the mushy zone that contains gas, liquid and solid is formed. The porosity – defined as the total volume of void, including the volumes of gas and liquid, relative to the total volume occupied by the solid matrix and void volume $[\varepsilon = (V_\ell + V_g)/(V_\ell + V_g + V_s) = \varphi_g + \varphi_\ell$; 25] – is constant in the lower part of the mushy zone. The whole powder bed shrinks as the interstitial gas between solid particles is driven out by the generated liquid phase. During the second stage, the upper part of the mushy zone that contains liquid and solid only is formed on top of the lower part of the mushy zone when the volume fraction of gas, φ_g, on the heating surface becomes zero. While shrinkage takes place in the lower part where the porosity remains constant, there is no shrinkage in the upper part if the densities of the solid and liquid phases of the powder material are the same. When the surface temperature of the powder bed reaches the liquidus temperature, the liquid region appears on top of the upper part of mushy zone and the process enters the third stage. During this stage, the powder bed is divided into four regions from the bottom to the heating surface: (1) unsintered region, (2) lower part of mushy zone with constant porosity (shrinkage takes place), (3) upper part of mushy zone with constant volume (no shrinkage), and (4) liquid region (see Fig. 1). The third stage of the melting represents the most complex situation and its governing equations and solutions are presented below.

2.1. Governing equations in different regions and interfaces

2.1.1. The unsintered region

The energy equation of the unsintered region underneath the mushy zone is

$$(\rho c)_p(1-\varepsilon)\frac{\partial T_s}{\partial t} = k_{eff}\frac{\partial^2 T_s}{\partial z^2}, \quad s(t) < z < \infty \tag{1}$$

where k_{eff} is the effective thermal conductivity in the unsintered region of the powder bed, which can be estimated using empirical correlation proposed by Hadley [26] for randomly packed spherical particles

$$k_{eff} = k_g(1-\alpha_0)\frac{\varepsilon f_0 + (k_p/k_g)(1-\varepsilon f_0)}{1-\varepsilon(1-f_0)+(k_p/k_g)\varepsilon(1-f_0)} + \alpha_0\frac{2(k_p/k_g)^2(1-\varepsilon)+(1+2\varepsilon)(k_p/k_g)}{(2+\varepsilon)(k_p/k_g)+1-\varepsilon} \tag{2}$$

where

$$f_0 = 0.8 + 0.1\varepsilon \tag{3}$$

$$\log\alpha_0 = \begin{cases} -4.898\varepsilon & 0 \leqslant \varepsilon \leqslant 0.0827 \\ -0.405 - 3.154(\varepsilon - 0.0827) & 0.0827 \leqslant \varepsilon \leqslant 0.298 \\ -1.084 - 6.778(\varepsilon - 0.298) & 0.298 \leqslant \varepsilon \leqslant 0.580 \end{cases} \tag{4}$$

2.1.2. The lower part of the mushy zone

The energy and continuity equations are

$$\frac{\partial(\rho c T_m)}{\partial t} + \frac{\partial(\rho c w T_m)}{\partial z} = \frac{\partial}{\partial z}\left(k\frac{\partial T_m}{\partial z}\right) + \rho h_{s\ell}\frac{\partial f}{\partial t}, \quad s_m(t) < z < s(t) \tag{5}$$

$$\frac{\partial\rho}{\partial t} + \frac{\partial(\rho w)}{\partial z} = 0, \quad s_m(t) < z < s(t) \tag{6}$$

Neglecting the contribution of gas to the density and heat capacity, the thermal properties of the lower part of the mushy zone can be expressed as

$$(\rho c)_{\mathrm{m}} = (1-\varphi_{\mathrm{g}})(\rho c)_{\mathrm{p}} \tag{7}$$

$$\rho_{\mathrm{m}} = (1-\varphi_{\mathrm{g}})\rho_{\mathrm{p}} \tag{8}$$

$$k_{\mathrm{m}} = (1-\varphi_{\mathrm{g}})k_{\mathrm{p}} \tag{9}$$

where the subscript p represents the properties of powder material. The thermal conductivity in the partially molten region, k_{m}, is much higher than that before melting because the contact area between the liquid and solid is significantly increased.

The degree of melting in the mushy zone can be measured by the solid fraction, f: a value of 1 indicates full solid, 0 indicates full liquid, and the value between 1 and 0 indicates mixture of solid and liquid. The solid fraction is related to the local temperature by

$$f = \begin{cases} 0 & T \geqslant T_{\ell \mathrm{m}} \\ \dfrac{T_{\ell \mathrm{m}} - T}{T_{\ell \mathrm{m}} - T_{\mathrm{sm}}} & T_{\mathrm{sm}} < T < T_{\ell \mathrm{m}} \\ 1 & T \leqslant T_{\mathrm{sm}} \end{cases} \tag{10}$$

The solid mass fraction, f, is related to the volume fractions of solid and liquid by

$$f = \frac{\rho_{\mathrm{ps}}\varphi_{\mathrm{s}}}{\rho_{\mathrm{ps}}\varphi_{\mathrm{s}} + \rho_{\mathrm{p}\ell}\varphi_{\ell}} \tag{11}$$

where ρ_{ps} and $\rho_{\mathrm{p}\ell}$ are densities of the solid and liquid phases of the powder material, which are assumed to be the same in the present study ($\rho_{\mathrm{ps}} = \rho_{\mathrm{p}\ell}$). At the lower part of the mushy zone, porosity in the mushy zone remains constant, so that always equals to $1-\varepsilon$. Eq. (11) can therefore be simplified as

$$f = \frac{1-\varepsilon}{1-\varphi_{\mathrm{g}}} \tag{12}$$

Substituting Eqs. (7)–(9) and Eq. (12) into Eqs. (5) and (6) the energy and continuity equations become

$$\frac{\partial}{\partial t}\left(\frac{T_{\mathrm{m}}}{f}\right) + \frac{\partial}{\partial z}\left(w\frac{T_{\mathrm{m}}}{f}\right) = \alpha_{\mathrm{p}}\frac{\partial}{\partial z}\left(\frac{1}{f}\frac{\partial T_{\mathrm{m}}}{\partial z}\right) + \frac{h_{s\ell}}{c_{\mathrm{p}}}\frac{1}{f}\frac{\partial f}{\partial t} \quad s_{\mathrm{m}}(t) < z < s(t) \tag{13}$$

$$\frac{\partial}{\partial t}\left(\frac{1}{f}\right) + \frac{\partial}{\partial z}\left(w\frac{1}{f}\right) = 0, \quad s_{\mathrm{m}}(t) < z < s(t) \tag{14}$$

2.1.3. The upper part of the mushy zone

The energy equation is

$$\frac{\partial T_{\mathrm{m}}}{\partial t} + w_0\frac{\partial T_{\mathrm{m}}}{\partial z} = \alpha_{\mathrm{p}}\frac{\partial^2 T_{\mathrm{m}}}{\partial z^2} + \frac{h_{s\ell}}{c_{\mathrm{p}}}\frac{\partial f}{\partial t}, \quad s_{\ell}(t) < z < s_{\mathrm{m}}(t) \tag{15}$$

Substituting Eq. (10) into Eq. (15), the energy equation in the upper part becomes

$$\left(1 + \frac{h_{s\ell}}{2c_{\mathrm{p}}\Delta T}\right)\frac{\partial T_{\mathrm{m}}}{\partial t} + w_0\frac{\partial T_{\mathrm{m}}}{\partial z} = \alpha_{\mathrm{p}}\frac{\partial^2 T_{\mathrm{m}}}{\partial z^2}, \quad s_{\ell}(t) < z < s_{\mathrm{m}}(t) \tag{16}$$

where $\Delta T = \mathrm{T}_{\ell \mathrm{m}} - T_{\mathrm{sm}}$ and $w_0 = \mathrm{d}s_0/\mathrm{d}t$.

2.1.4. The liquid region

The energy equation is

$$\frac{\partial T_{\ell}}{\partial t} + w_0\frac{\partial T_{\ell}}{\partial z} = \alpha_{\mathrm{p}}\frac{\partial^2 T_{\ell}}{\partial z^2}, \quad s_0(t) < z < s_{\ell}(t) \tag{17}$$

which is subject to the following boundary condition

$$k_{\mathrm{p}}\frac{\partial T_{\ell}}{\partial z} = -q'', \quad z = s_0(t) \tag{18}$$

2.1.5. Interfacial boundary conditions

The temperature at the interface between the mushy zone and unsintered regions is equal to the solidus temperature, i.e.,

$$T_{\mathrm{s}} = T_{\mathrm{m}} = T_{\mathrm{sm}}, \quad z = s(t) \tag{19}$$

and the energy balance at the interface between mushy zone and unsintered regions is

$$k_{\mathrm{p}}(1-\varepsilon)\frac{\partial T_{\mathrm{m}}}{\partial z} = k_{\mathrm{eff}}\frac{\partial T_{\mathrm{s}}}{\partial z}, \quad z = s(t) \tag{20}$$

At the interface between the upper and lower parts of the mushy zone, the volume fraction of the gas, φ_{g}, is zero and the solid fraction, f, is equal to $1-\varepsilon$ according to Eq. (12). Therefore, the temperature at the interface between the upper and lower parts can be obtained from Eq. (10), i.e.,

$$T_{\mathrm{m}} = T_{\mathrm{sm}} + \varepsilon(T_{\ell \mathrm{m}} - T_{\mathrm{sm}}), \quad z = s_{\mathrm{m}}(t) \tag{21}$$

The energy balance at the interface of the upper and lower parts of mushy zone is

$$\left.\frac{\partial T_{\mathrm{m}}}{\partial z}\right|_{z=s_{\mathrm{m}}^{+}} = \left.\frac{\partial T_{\mathrm{m}}}{\partial z}\right|_{z=s_{\mathrm{m}}^{-}}, \quad z = s_{\mathrm{m}}(t) \tag{22}$$

The temperature at the interface between mushy zone and liquid region is equal to the liquidus temperature

$$T_{\ell} = T_{\mathrm{m}} = T_{\ell \mathrm{m}}, \quad z = s_{\ell}(t) \tag{23}$$

The energy balance at the interface between mushy and liquid zones is

$$\frac{\partial T_{\ell}}{\partial z} = \frac{\partial T_{\mathrm{m}}}{\partial z}, \quad z = s_{\ell}(t) \tag{24}$$

3. Non-dimensional governing equations

Introducing the following dimensionless variables

$$\begin{aligned} \tau &= \frac{\alpha_{\mathrm{p}}t}{(\alpha_{\mathrm{p}}\rho_{\mathrm{p}}h_{s\ell}/q'')^2}, \quad \theta = \frac{c_{\mathrm{p}}(T - T_{\ell \mathrm{m}})}{h_{s\ell}}, \\ Z &= \frac{z}{\alpha_{\mathrm{p}}\rho_{\mathrm{p}}h_{s\ell}/q''}, \quad S = \frac{s}{\alpha_{\mathrm{p}}\rho_{\mathrm{p}}h_{s\ell}/q''}, \\ W &= \frac{w\alpha_{\mathrm{p}}\rho_{\mathrm{p}}h_{s\ell}/q''}{\alpha_{\mathrm{p}}}, \quad W_0 = \frac{w_0\alpha_{\mathrm{p}}\rho_{\mathrm{p}}h_{s\ell}/q''}{\alpha_{\mathrm{p}}}, \\ K_{\mathrm{eff}} &= \frac{k_{\mathrm{eff}}}{k_{\mathrm{p}}(1-\varepsilon)}, \quad \delta\theta = \frac{c_{\mathrm{p}}(T_{\ell \mathrm{m}} - T_{\mathrm{sm}})}{h_{s\ell}} \end{aligned} \tag{25}$$

the governing equations and boundary conditions can be nondimensionalized as follows:

$$K_{\text{eff}}\frac{\partial^2\theta_s}{\partial Z^2}=\frac{\partial\theta_s}{\partial\tau},\quad S(\tau)<Z<\infty \tag{26}$$

$$\frac{\partial}{\partial\tau}\left(\frac{\theta_m}{f}\right)+\frac{\partial}{\partial Z}\left(W\frac{\theta_m}{f}\right)=\frac{\partial}{\partial Z}\left(\frac{1}{f}\frac{\partial\theta_m}{\partial Z}\right)+\frac{1}{f}\frac{\partial f}{\partial\tau},\quad S_m(\tau)<Z<S(\tau) \tag{27}$$

$$\frac{\partial}{\partial\tau}\left(\frac{1}{f}\right)+\frac{\partial}{\partial Z}\left(\frac{W}{f}\right)=0,\quad S_m(\tau)<Z<S(\tau) \tag{28}$$

$$\left(1+\frac{1}{\delta\theta}\right)\frac{\partial\theta_m}{\partial\tau}+W_0\frac{\partial\theta_m}{\partial Z}=\frac{\partial^2\theta_m}{\partial Z^2},\quad S_\ell(\tau)<Z<S_m(\tau) \tag{29}$$

$$\frac{\partial^2\theta_\ell}{\partial Z^2}=\frac{\partial\theta_\ell}{\partial\tau}+W_0\frac{\partial\theta_\ell}{\partial Z},\quad S_0(\tau)<Z<S_\ell(\tau) \tag{30}$$

$$\frac{\partial\theta_\ell}{\partial Z}=-\frac{1}{1-\varepsilon},\quad Z=S_0(\tau) \tag{31}$$

$$\theta_s=\theta_m=-\delta\theta,\quad Z=S(\tau) \tag{32}$$

$$K_{\text{eff}}\frac{\partial\theta_s}{\partial Z}=\frac{\partial\theta_m}{\partial Z},\quad Z=S(\tau) \tag{33}$$

$$\theta_m=(\varepsilon-1)\delta\theta,\quad Z=S_m(\tau) \tag{34}$$

$$\left.\frac{\partial\theta_m}{\partial Z}\right|_{Z=S_m^+}=\left.\frac{\partial\theta_m}{\partial Z}\right|_{Z=S_m^-},\quad Z=S_m(\tau) \tag{35}$$

$$\theta_\ell=\theta_m=0,\quad Z=S_\ell(\tau) \tag{36}$$

$$\frac{\partial\theta_\ell}{\partial Z}=\frac{\partial\theta_m}{\partial Z},\quad Z=S_\ell(\tau) \tag{37}$$

4. Integral approximate solutions

The integral approximate method for unsintered region requires introduction of the dimensionless thermal penetration depth, Δ, beyond which the temperature of the powder bed is not affected by the surface heating, i.e.,

$$\theta_s(\Delta,\tau)=0 \tag{38}$$

$$\frac{\partial\theta_s(\Delta,\tau)}{\partial Z}=0 \tag{39}$$

The integral equation of unsintered region is obtained by integrating Eq. (26) in the interval of (S,Δ) with respect to Z:

$$K_{\text{eff}}\left[\frac{\partial\theta(\Delta,\tau)}{\partial Z}-\frac{\partial\theta(S,\tau)}{\partial Z}\right]=\frac{d}{d\tau}\left(\int_S^\Delta\theta dZ-\theta_i\Delta-\delta\theta S\right) \tag{40}$$

Assuming a second degree polynomial temperature distribution in the unsintered region and using Eqs. (32), (38) and (39) to determine the constants, the temperature distribution in the unsintered region is obtained

$$\theta_s(Z,\tau)=\theta_i-(\theta_i+\Delta\theta_m)\left(\frac{\Delta-Z}{\Delta-S}\right)^2 \tag{41}$$

Substituting Eq. (41) into Eq. (40), one obtains the following differential equation for thermal penetration depth and the interface between the unsintered region and mushy zone

$$\frac{6K_{\text{eff}}}{\Delta-S}=\frac{d\Delta}{d\tau}+2\frac{dS}{d\tau} \tag{42}$$

The integral equations in the lower part of the mushy zone are obtained by integrating Eqs. (27) and (28) from S_m to S with respect to Z:

$$\frac{d}{d\tau}\left(\int_{S_m}^S\frac{\theta_m}{f}dZ-\int_{S_m}^S(\ln f)dZ-\left.\frac{\theta_m}{f}\right|_{Z=S}S-\ln f|_{Z=S_m}S_m\right)=\left.\frac{1}{f}\frac{\partial\theta_m}{\partial Z}\right|_{S_m}^S \tag{43}$$

$$\frac{d}{d\tau}\left(\int_{S_m}^S\frac{1}{f}dz-\left.\frac{1}{f}\right|_{Z=S}S+\left.\frac{1}{f}\right|_{Z=S_m}S_m\right)+\left.\frac{W}{f}\right|_{S_m}^S=0 \tag{44}$$

The expression of solid fraction, f, as a single value of temperature in the lower part of the mushy zone defined in Eq. (10), is difficult to be used in Eqs. (43) and (44) because of the complexity of the integral equations. The effect of the distribution of the solid fraction in the mushy zone using the integral method was investigated by Tien and Geiger [27], who concluded that the result deviations are only four to eight percent when different forms of solid fraction distributions were used. For the ease of integration, the inverse of solid fraction is assumed to be a linear function of in the mushy zone, i.e.,

$$\frac{1}{f}=1+\frac{\varepsilon}{1-\varepsilon}\frac{S-Z}{S-S_m} \tag{45}$$

It is also assumed that temperature distribution in the lower part of the mushy zone is a second degree polynomial function

$$\frac{\theta_m}{f}=B_0+B_1\left(\frac{S-Z}{S-S_m}\right)+B_2\left(\frac{S-Z}{S-S_m}\right)^2,\quad S_m(\tau)<Z<S(\tau),\tau>\tau_\ell \tag{46}$$

where the constants, B_0, B_1 and B_2 can be obtained by using the boundary conditions specified by Eqs. (32)–(34):

$$B_0=-\delta\theta \tag{47}$$

$$B_1=-\frac{\varepsilon}{1-\varepsilon}\delta\theta-\frac{2K_{\text{eff}}(\theta_i+\delta\theta)(S-S_m)}{\Delta-S} \tag{48}$$

$$B_2=\frac{\varepsilon}{1-\varepsilon}\delta\theta+\frac{2K_{\text{eff}}(\theta_i+\delta\theta)(S-S_m)}{\Delta-S} \tag{49}$$

Substituting Eqs. (45)–(49) into Eqs. (43) and (44), one obtains

$$S_m=\frac{2}{\varepsilon}S_0-S \tag{50}$$

$$\frac{d}{d\tau}\left(-\frac{K_{\text{eff}}(\theta_i+\delta\theta)}{3(\Delta-S)}(S-S_m)^2-\left(\frac{\varepsilon\delta\theta}{6(1-\varepsilon)}+1+\frac{\ln(1-\varepsilon)}{\varepsilon}\right)(S-S_m)\right)+\delta\theta\frac{dS_0}{d\tau}-\ln(1-\varepsilon)\frac{dS_m}{d\tau}=\frac{4K_{\text{eff}}(\theta_i+\delta\theta)}{\Delta-S}+\frac{\varepsilon(2-\varepsilon)\delta\theta}{(1-\varepsilon)(S-S_m)} \tag{51}$$

Integrating Eq. (29) in the interval of (S_ℓ,S_m) with respect to Z, the integral equation for the upper part of the mushy zone becomes

$$\left(1+\frac{1}{\delta\theta}\right)\left[\frac{\mathrm{d}}{\mathrm{d}\tau}\int_{S_\ell}^{S_m}\theta_m\,\mathrm{d}Z-(\varepsilon-1)\delta\theta\frac{\mathrm{d}S_m}{\mathrm{d}\tau}\right]+W_0[(\varepsilon-1)\delta\theta]=\left.\frac{\partial\theta_m}{\partial Z}\right|_{Z=S_m}-\left.\frac{\partial\theta_m}{\partial Z}\right|_{Z=S_\ell} \tag{52}$$

Assuming the temperature distribution in the upper part of the mushy zone as a second degree polynomial function and applying the boundary conditions of Eqs. (34)–(36) yields

$$\theta_m=(\varepsilon-1)\delta\theta+D_m(S_m-Z)+[(1-\varepsilon)\delta\theta-D_m(S_m-S_\ell)]\left(\frac{S_m-Z}{S_m-S_\ell}\right)^2 \tag{53}$$

where

$$D_m=\frac{\varepsilon(2-\varepsilon)\delta\theta}{S-S_m}+\frac{2K_{eff}(\theta_i+\delta\theta)(1-\varepsilon)}{\Lambda-S} \tag{54}$$

Substituting Eq. (53) into Eq. (52) yields

$$\left(1+\frac{1}{\delta\theta}\right)\frac{\mathrm{d}}{\mathrm{d}\tau}\left[\frac{1}{6}D_m(S_m-S_\ell)^2+\frac{(1-\varepsilon)\delta\theta}{3}(4S_m-S_\ell)\right]-(1-\varepsilon)\delta\theta\frac{\mathrm{d}S_0}{\mathrm{d}\tau}=\frac{2(1-\varepsilon)\delta\theta}{S_m-S_\ell}-2D_m \tag{55}$$

Since the entire liquid layer moves with the velocity W_0, the layer is stationary from the coordinate Z' that moves with velocity W_0. The relationship between the two coordinate systems is

$$Z'=Z-\int_{\tau_\ell}^{\tau}W_0\,\mathrm{d}\tau=Z-S_0 \tag{56}$$

The energy equation and the corresponding boundary conditions can be rewritten as

$$\frac{\partial^2\theta_\ell}{\partial Z'^2}=\frac{\partial\theta_\ell}{\partial\tau},\quad 0<Z'<S_\ell-S_0,\quad \tau>\tau_\ell \tag{57}$$

$$\frac{\partial\theta_\ell}{\partial Z'}=-\frac{1}{1-\varepsilon},\quad Z'=0,\quad \tau>\tau_\ell \tag{58}$$

$$\theta_\ell(Z',\tau)=0,\quad Z'=S_\ell-S_0,\quad \tau>\tau_\ell \tag{59}$$

The exact solution of Eqs. (57)–(59) is [28]

$$\theta'_\ell(Z',\tau)=\frac{2\sqrt{\tau-\tau_\ell}}{1-\varepsilon}\left[\mathrm{ierfc}\left(\frac{Z'}{2\sqrt{\tau-\tau_\ell}}\right)-\mathrm{ierfc}\left(\frac{S_\ell-S_0}{2\sqrt{\tau-\tau_\ell}}\right)\right] \tag{60}$$

Changing back to the Z coordinate system, Eq. (60) can be rewritten as

$$\theta_\ell(Z,\tau)=\frac{2\sqrt{\tau-\tau_\ell}}{1-\varepsilon}\left[\mathrm{ierfc}\left(\frac{Z-S_0}{2\sqrt{\tau-\tau_\ell}}\right)-\mathrm{ierfc}\left(\frac{S_\ell-S_0}{2\sqrt{\tau-\tau_\ell}}\right)\right] \tag{61}$$

Substituting Eqs. (53) and (61) into Eq. (37), the energy balance at the interface between the liquid region and the mushy zone becomes

$$\frac{1}{1-\varepsilon}\mathrm{erfc}\left(\frac{S_\ell-S_0}{2\sqrt{\tau-\tau_\ell}}\right)=\frac{2(1-\varepsilon)\delta\theta}{S_m-S_\ell}-D_m \tag{62}$$

Eqs. (42), (50), (51), (55) and (62) can be solved by the fourth order Runge–Kutta method with the initial conditions obtained from the solutions of melting at the second melting stage.

5. Result and discussion

Laser melting of nickel braze (BNi-2) powders – with a melting temperature range from 971 °C (solidus) to 999 °C (liquidus) [29] – will be studied to demonstrate the capability of the model developed in this study. Nickel braze is chosen because it is a commonly used mould material for its high strength and heat resistance to corrosion. The thermophysical properties of Nickel braze used in the calculations are shown in Table 1 [29,30]. The effects of initial porosity, subcooling and thermal conductivity of the interstitial gas will be examined.

The initial porosity or the initial volume fraction of the gas is directly related to the shape and arrangements of the powders particles. For spherical powder particles, simple-cubic (6 contact points), body-centered cubic (8 contact points), face-centered cubic (12 contact points) arrangements correspond to the porosity of 0.476, 0.32, 0.264, respectively [31]. When the spherical particles are randomly packed, the porosity is about 0.4. Fig. 2 shows the evolution of surface temperature for different initial porosities during the melting process. The surface temperature increases rapidly during the preheating stage due to low

Table 1
Thermophysical properties of nickel braze

Properties	Symbol	Unit	Value
Density	ρ_p	kg/m^3	8257
Thermal conductivity	k_p	W/m K	14.65
Specific heat	c_p	J/kg K	462.6
Solidus temperature	T_{sm}	°C	971
Liquidus temperature	$T_{\ell m}$	°C	999
Latent heat of fusion	$h_{s\ell}$	kJ/kg	377.4

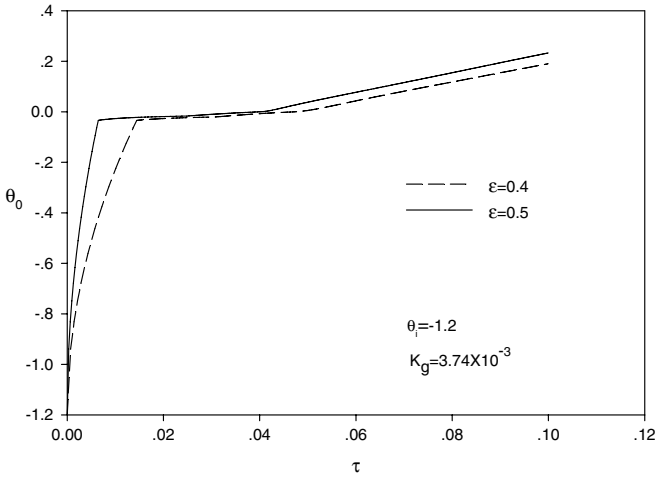

Fig. 2. Surface temperature for different initial porosities.

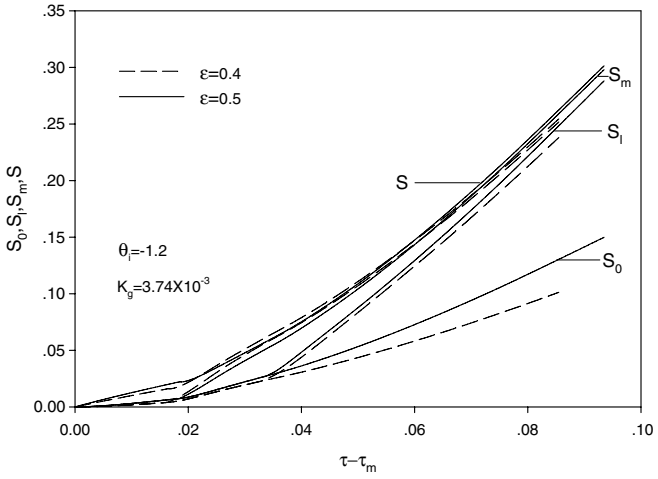

Fig. 3. Interfacial locations for different initial porosities.

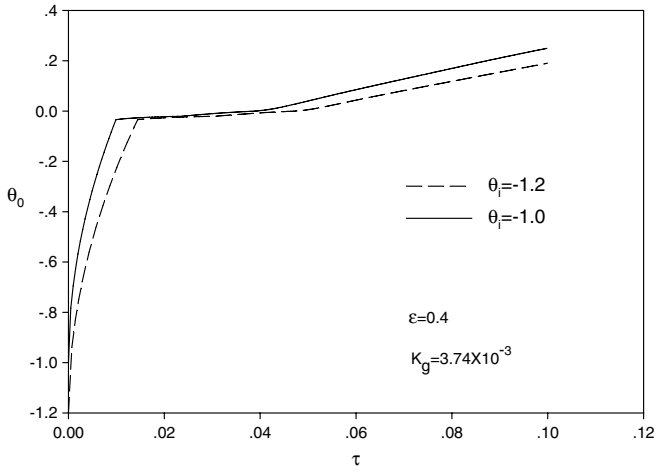

Fig. 5. Surface temperature for different subcooling parameters.

thermal conductivity of the loose powders. After the surface temperature reaches to the solidus temperate, melting occurs and the surface temperature increases slowly. Once the surface temperature reaches to the liquidus temperature, a liquid region is formed and the increasing of the surface temperature becomes faster. Due to lower effective thermal conductivity with higher porosity, the surface temperature increases and the duration of preheating is shortened when the initial porosity increases.

Fig. 3 shows the evolution of various interfacial locations corresponding to the same conditions as Fig. 2. The motion of solid-mushy interface (S_ℓ) is faster than that of heating surface (S_0) at the beginning. After the upper part of the mushy zone is formed, the solid-mushy interface moves downward rapidly due to higher thermal conductivity in the upper part. After the liquid region is formed, the liquid-mushy interfacial velocity is faster than the interfacial velocities between two parts of mushy zone, which narrows the thickness of the whole mushy zone. Melting accelerates with increasing initial porosity because higher porosity means lower density and thermal conductivity in the unsintered region. Fig. 4 shows the evolution of solid fraction on the surface ($X = S_0$) of the powder bed corresponding to the same conditions as Fig. 2. The solid fraction on the surface decreases slowly before the upper part of the mushy zone is formed. Upon formation of the upper part, the solid fraction on the heating surface decreases rapidly. When initial porosity increases, the decreasing rate of the solid fraction at the heating surface increases before the upper part is formed. After the upper part is formed, the decreasing rate of the solid fraction at the heating surface slows down slightly when initial porosity increases.

Fig. 5 shows the evolution of surface temperature for different subcooling parameters (or initial temperatures). When initial temperature decreases, the duration of the preheating increases and surface temperature increases. Fig. 6 shows the evolution of interfacial locations corresponding to the same conditions as Fig. 5. The interfacial velocities increase with increasing subcooling parameter. Fig. 7 shows the evolution of solid fraction on the heating

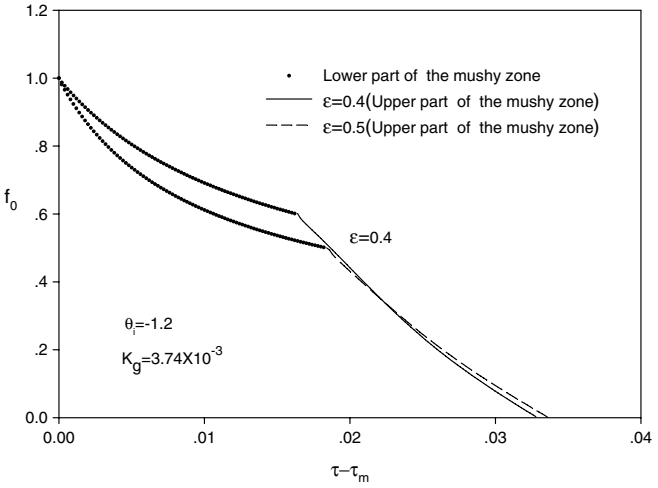

Fig. 4. Solid fraction on the heating surface for different initial porosities.

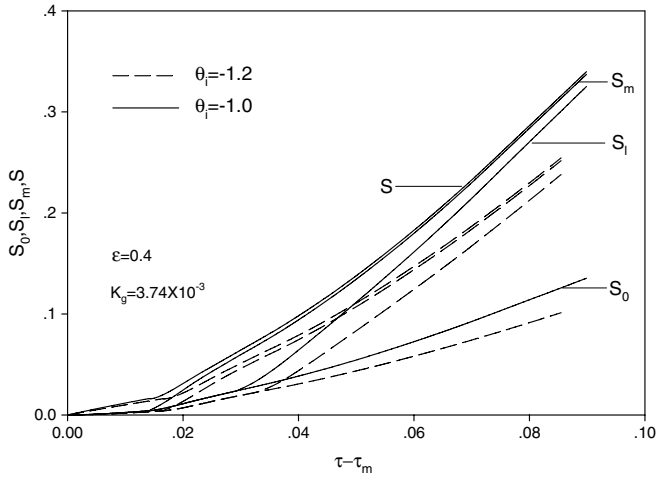

Fig. 6. Interfacial locations for different subcooling parameters.

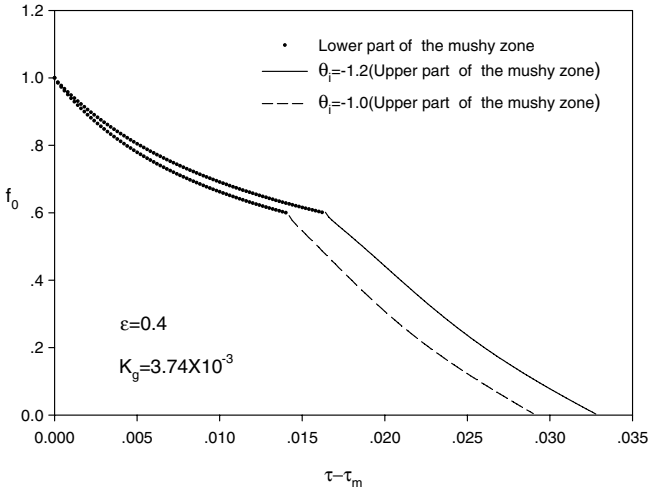

Fig. 7. Solid fraction on the heating surface for different subcooling parameters.

surface corresponding to the same conditions as Fig. 5. It can be seen that the decreasing rate of the solid fraction at the heating surface decreases with increasing subcooling parameter.

Dimensionless thermal conductivity of the gas is a key factor of the effective thermal conductivity in the unsintered regions [see Eq. (2)] which has significant effect on the sintering process. Fig. 8 shows the evolution of surface temperature for different dimensionless thermal conductivities of the gas. It can be seen that the preheating time increases significantly when the thermal conductivity of the gas is increased because more heat is conducted into the powder bed due to higher effective thermal conductivity in the unsintered zone. Fig. 9 shows the evolution of interfacial locations corresponding to the same conditions as Fig. 8. The increase of dimensionless thermal conductivity of the gas does not have significant influence on the thickness of mushy zone. The moving velocities of the interfaces for the higher thermal conductivity of the interstitial gases

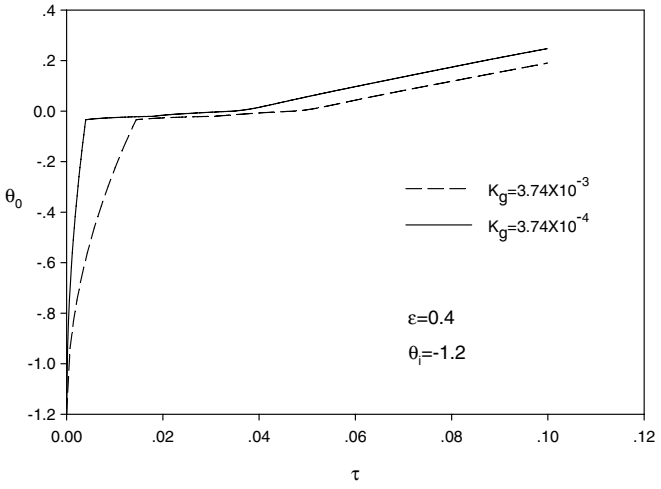

Fig. 8. Surface temperature for different thermal conductivities of the interstitial gas.

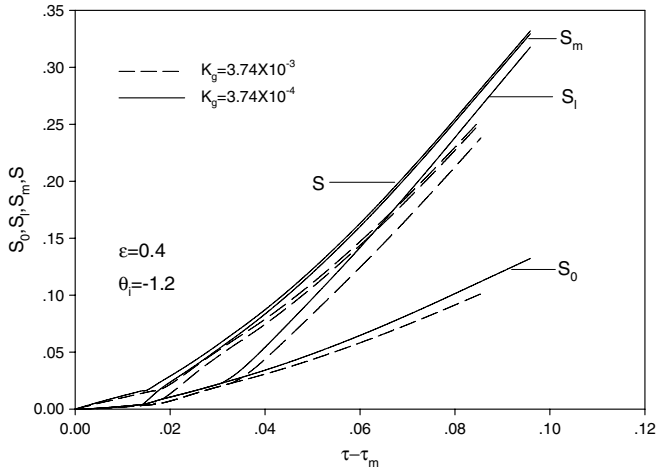

Fig. 9. Interfacial locations for different thermal conductivities of the interstitial gas.

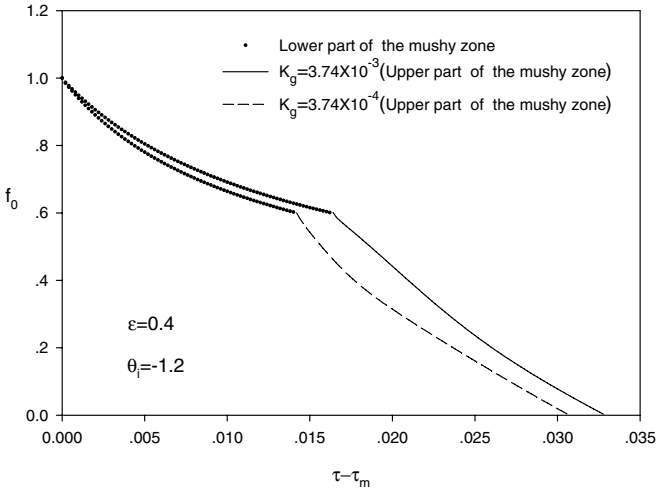

Fig. 10. Solid fraction on the heating surface for different thermal conductivities of the interstitial gas.

are faster than those for the lower thermal conductivity of the interstitial gases. Fig. 10 shows the evolution of the solid fraction on the heating surface corresponding to the same conditions as Fig. 8. It can be seen that the decreasing rate of the solid fraction before upper part of the mushy zone is formed decreases with increasing thermal conductivity of the gas. The decreasing rate of the solid fraction after formation of the upper part increases slightly with increasing thermal conductivity of the gas.

6. Conclusion

Melting of an alloy powder bed with shrinkage is investigated analytically. Effects of various processing parameters on the surface temperature, interfacial locations and solid fraction on the surface were investigated. Increasing initial porosity of the powder bed shortens the duration of preheating, increases the surface temperature and inter-

facial velocities, and accelerates the decrease of solid fraction on the heating surface. Increasing subcooling parameter has similar effect on the sintering process with increasing porosity. On the contrary, increasing thermal conductivity of the gas, decreases the interfacial velocities and surface temperature, and decelerates the decrease of solid fraction on the heating surface.

Acknowledgement

Support for this work by the Office of Naval Research (ONR) under Grant Number N00014-04-1-0303 is gratefully acknowledged.

References

[1] M. Agarwala, D. Bourell, J. Beaman, H. Marcus, J. Barlow, Direct selective laser sintering of metals, Rapid Prototyping J. 1 (1) (1995) 26–36.
[2] J.G. Conley, H.L. Marcus, Rapid prototyping and solid free form fabrication, ASME J. Manufacturing Sci. Eng. 119 (4) (1997) 811–816.
[3] R. Morgan, C.J. Sutcliffe, W. O'Neill, Experimental investigation of nanosecond pulsed Nd:YAG laser Re-melted pre-placed powder beds, Rapid Prototyping J. 7 (3) (2001) 159–172.
[4] S. Kumar, Selective laser sintering: a qualitative and objective approach, JOM 55 (10) (2003) 43–47.
[5] F. Abe, E. Costa Santos, Y. Kitamura, K. Osakada, M. Shiomi, Influence of forming conditions on the titanium model in rapid prototyping with the selective laser melting process, Proc. Inst. Mech. Eng. Part C – J. Mech. Eng. Sci. 217 (1) (2003) 119–126.
[6] R. Viskanta, Phase change heat transfer, in: G.A. Lane (Ed.), Solar Heat Storage: Latent Heat Materials, CRC Press, Boca Raton, FL, 1983.
[7] L.S. Yao, J. Prusa, Melting and freezing, Adv. Heat Transfer 19 (1989) 1–95.
[8] A. Faghri, Y. Zhang, Transport Phenomena in Multiphase Systems, Elsevier, Burlington, MA, 2006.
[9] H.S. Carslaw, J.C. Jaeger, Conduction of Heat in Solids, Clarendon Press, Oxford, 2006.
[10] M. Lax, Temperature rise induced by a laser beam, J. Appl. Phys. 48 (9) (1977) 3919–3924.
[11] A.E. Bell, Review and analysis of laser annealing, RCA Rev. 42 (3) (1979) 295–298.
[12] B.S. Yilbas, Study into a numerical solution for a pulsed CO_2 laser heating process, Numer. Heat Transfer A 28 (4) (1995) 487–502.
[13] A.A. Rostaml, A. Raisi, Temperature distribution and melt pool size in a semi-infinite body due to a moving laser heat source, Numer. Heat Transfer A 31 (7) (1997) 783–796.
[14] W.S. Kim, B.C. Sim, Study of thermal behavior and fluid flow during laser surface heating of alloys, Numer. Heat Transfer A 31 (7) (1997) 703–723.
[15] M. Iwamoto, M. Ye, C.P. Grigoropoulos, R. Grief, Numerical analysis of pulsed laser heating for the deformation of metals, Numer. Heat Transfer A 34 (8) (1998) 791–804.
[16] J.K. Chen, J.E. Beraun, Numerical study of ultrashort laser pulse interactions with metal films, Numer. Heat Transfer A 40 (1) (2001) 1–20.
[17] I.H. Chowdhury, X. Xu, Heat transfer in femtosecond laser processing of metal, Numer. Heat Transfer A 44 (3) (2003) 219–232.
[18] F.B. Hsiao, D.B. Wang, C.P. Jen, Numerical investigation on thermal contact resistance between the mold and substrate on laser-assisted imprinting fabrication, Numer. Heat Transfer A 49 (7) (2006) 669–682.
[19] E.R.G. Eckert, R.M. Drake, Analysis of Heat and Mass Transfer, McGraw-Hill, London, 1972.
[20] Y. Zhang, A. Faghri, Melting of a subcooled mixed powder bed with constant heat flux heating, Int. J. Heat Mass Transfer 42 (5) (1999) 775–788.
[21] C. Konrad, Y. Zhang, B. Xiao, Analysis of melting and resolidification in a two-component metal powder bed subjected to temporal Gaussian heat flux, Int. J. Heat Mass Transfer 48 (19–20) (2005) 3932–3944.
[22] B. Xiao, Y. Zhang, Analysis of partial melting in a metal powder bed with constant heat flux, Heat Transfer Eng. 28 (5) (2007), to appear.
[23] H.J. Niu, I.T.H. Chang, Liquid phase sintering of M3/2 high speed steel by selective laser sintering, Scripta Mater. 39 (1) (1998) 67–72.
[24] G. Prabhu, D.L. Bourell, Supersolidus liquid phase sintering of prealloyed bronze powder, in: J.J. Beaman, H.L. Marcus, D.L. Bourell, J.W. Barlow (Eds.), Proceedings of the Solid Freeform Fabrication Symposium, The University of Texas at Austin, Austin, TX, 1993, pp. 317–324.
[25] J. Pak, O.A. Plumb, Melting in a two-component packed bed, ASME J. Heat Transfer 119 (3) (1997) 553–559.
[26] G.R. Hadley, Thermal conductivity of packed metal powders, Int. J. Heat Mass Transfer 29 (6) (1986) 909–920.
[27] R.H. Tien, G.E. Geiger, A heat-transfer analysis of the solidification of a binary eutectic system, ASME J. Heat Transfer 89 (3) (1967) 230–234.
[28] M.S. El-Genk, A.W. Cronenberg, Solidification in a semi-infinite region with boundary condition of the second kind: an exact solution, Lett. Heat Mass Transfer 6 (4) (1979) 321–327.
[29] The brazing book, Handy and Harman, New York, 2001. <http://www.brazingbook.com>.
[30] Y. Zhang, Thermal modeling of advanced manufacturing technologies: grinding, laser drilling, and solid freeform fabrication, Ph.D. Thesis, University of Connecticut, Storrs, CT, 1998.
[31] M. Kaviany, Principles of Heat Transfer in Porous Media, second ed., Springer-Verlag, New York, 1997.